

# Electromagnetic Afterglows Associated with Gamma-Ray Emission Coincident with Binary Black Hole Merger Event GW150914

Ryo Yamazaki<sup>1</sup>, Katsuaki Asano<sup>2</sup>, Yutaka Ohira<sup>1</sup>

<sup>1</sup>*Department of Physics and Mathematics, Aoyama Gakuin University, 5-10-1 Fuchinobe, Sagamihara 252-5258, Japan*

<sup>2</sup>*Institute for Cosmic Ray Research, The University of Tokyo, 5-1-5 Kashiwanoha, Kashiwa, Chiba 277-8582, Japan*

## ABSTRACT

Fermi Gamma-ray Burst Monitor detected gamma-ray emission 0.4 sec after a binary black-hole merger event, GW150914. We show that the gamma-ray emission is caused by a relativistic outflow with Lorentz factor larger than 10. Subsequently debris outflow pushes ambient gas to form a shock, which is responsible for the afterglow synchrotron emission. We find that the fluxes of radio and optical afterglows increase from about  $10^7$  sec to at least  $\sim 10$  yr after the burst trigger. Further follow-up observations in the radio and optical/infrared bands are encouraged. Detection of afterglows will localize the sky position of the gravitational-wave and the gamma-ray emissions and it will support the physical association between them.

*Subject headings:* gamma-ray burst: general — gravitational waves

## 1. Introduction

On September 14, 2015 Laser Interferometer Gravitational-Wave Observatory (LIGO) detected a transient gravitational wave (GW) signal of a binary black hole (BH) merger (Abbott et al. 2016). Analysis of this event, GW150914, showed that energy of  $\sim 3M_\odot c^2$  went into GWs and that the luminosity distance to the source was  $\approx 410$  Mpc, corresponding to a redshift of  $z \approx 0.09$  (Abbott et al. 2016; LIGO Scientific Collaboration and Virgo Collaboration 2016). LIGO provided us direct evidence for existence of binary BH systems and even existence of intermediate-mass BHs. This is the beginning of GW astronomy.

It is also surprising that *Fermi* Gamma-ray Burst Monitor (GBM) detected a weak gamma-ray emission 0.4 sec after the detection of GW150914 (Connaughton et al. 2016).

The gamma-ray emission lasted for about 0.1 sec. The observed fluence between 10 and 1000 keV is  $2\text{--}3 \times 10^{-7} \text{ erg cm}^{-2}$ , so that the isotropic-equivalent gamma-ray energy  $E_\gamma$  is  $5 \times 10^{48} \text{ erg}$ , which is only a small fraction ( $\sim 10^{-6}$ ) of the energy radiated by GW. The gamma-ray luminosity in 1 keV–10 MeV band is measured as  $L_\gamma = 1.8 \times 10^{49} \text{ erg s}^{-1}$ , which is again very tiny fraction of GW luminosity of  $\sim 10^{55} \text{ erg s}^{-1}$  ( $\sim 10^{-4}c^5/G$ ). A possible peak energy in the spectrum is a few MeV, and there is no evidence of photons above  $\sim 5 \text{ MeV}$ . So far, no other electromagnetic counterpart emission has been reported (Annis et al. 2016; Evans et al. 2016; Fermi LAT Collaboration 2016; Soares-Santos et al. 2016; Savchenko et al. 2016; Smartt et al. 2016).

In this paper, we point out that the gamma-ray emission coincident with GW150914 arises from relativistically expanding material with the bulk Lorentz factor larger than 10 (section 2). Then, we consider the afterglow emission which is a synchrotron emission of relativistic electrons accelerated at a shock propagating into the ambient matter (section 3). Finally, in section 4, we compare our model prediction with current upper limits in X-ray, optical, infrared, and radio bands. Throughout this paper, we use the “TT+lowP+lensing+ext” cosmological parameters from Table 4 of Planck Collaboration et al. (2015).

## 2. Gamma-ray Emission

The horizon scale of the final BH, whose mass  $M_{\text{BH}} = 62M_\odot$  and spin parameter  $a = 0.7$ , is  $R_{\text{BH}} = (1 + \sqrt{1 - a^2})GM_{\text{BH}}/c^2 \sim 1.6 \times 10^7 \text{ cm}$ . If the energy source of the gamma-ray emission is the gravitational energy of accreting matter, the required mass is  $M_{\text{acc}} \sim E_\gamma R_{\text{BH}}/(GM_{\text{BH}}) \sim 10^{-5}M_{\text{sun}}$  for  $E_\gamma \sim 10^{49} \text{ erg}$ . The required mass is so tiny compared to  $M_{\text{BH}}$  that it is not surprising even if a small part of the circum-binary disk supplies such a small mass  $M_{\text{acc}}$  onto the BH. Another possible way of the energy release is the dissipation of the magnetic energy  $\sim B^2 R_{\text{BH}}^3/6$ , which implies  $B \sim 1.2 \times 10^{14} \text{ G}$ . Alternatively, the Blandford-Znajek (BZ) process may extract the rotation energy of the BH (Blandford & Znajek 1977) and produce Poynting flux dominated jets. The required magnetic field is  $B \sim \sqrt{L_\gamma/(ca^2 R_{\text{BH}}^2)} \sim 1.7 \times 10^{12} \text{ G}$  for  $L_\gamma \sim 10^{49} \text{ erg s}^{-1}$ .

First, let us consider the fireball model (Shemi & Piran 1990), which has been applied for gamma-ray bursts (GRBs). A prompt energy release in the localized region around the BH leads to an optically-thick radiation-dominated plasma, whose components are photons, electrons and positrons, with the energy density  $e_0 = 3E_\gamma/(4\pi R_{\text{BH}}^3)$ . The initial temperature is calculated as  $T_0 = (60\hbar^3 c^3 e_0/11\pi^2)^{1/4} \sim 1.1 \text{ MeV}$ . The fireball starts to expand and is accelerated by its own pressure; the Lorentz factor grows with the radius as  $\Gamma \propto R$  and the temperature drops as  $T' \propto R^{-1}$  (the photon energy density  $e' \propto T'^4 \propto R^{-4}$ )

(Piran, Shemi & Narayan 1993). The photon temperature for the observer  $T_{\text{obs}} = \Gamma T' = T_0$  is constant, and consistent with the observed spectrum. The number density of the electron–positron pairs in the complete thermal equilibrium decreases with temperature as  $n'_{\pm} = 4(m_e T' / 2\pi\hbar^2)^{3/2} \exp(-m_e c^2 / T')$ . In the baryon-free limit, the photosphere radius, where  $n'_{\pm} \sigma_T R / \Gamma = 1$ , is calculated as  $R_{\text{ph}} = 59 R_{\text{BH}}$ , which means  $\Gamma = 59$  at the photosphere. The luminosity of the photospheric emission is  $L_{\gamma} = 4\pi c R_{\text{ph}}^2 \Gamma^2 e' \simeq 3cE_{\gamma}/R_{\text{BH}} \sim 5.7 \times 10^{52}$  erg s<sup>−1</sup>, which is much higher than the observed value. Even for the trapped fireball model (Thompson & Duncan 1995), in which the fireball is trapped in the magnetosphere of the BH, the situation for the luminosity is the same.

Therefore, the observed gamma-ray emission is not due to the photospheric emission from the baryon-free fireball. The fireball may be contaminated by baryons. In such a case, the fireball expansion evolves to a relativistic outflow of baryons, which may emit gamma-rays at outer radius via internal shock etc. (Piran 1999) or relic thermal photons at the baryonic photosphere. If the observed emission is coming from the baryonic photosphere, a much more energy is required as the bulk kinetic energy of the baryons. The maximum gamma-ray energy is a few MeV in the observation. If the bulk Lorentz factor is higher than 10, the energies of those photons are below  $m_e c^2$  in the comoving frame of the outflow. Then, the electron-positron pair production in the source can be avoided so that gamma-rays can safely escape from the source. Therefore, the observed gamma-ray emission may require a relativistic baryonic/magnetic outflow with the bulk Lorentz factor larger than 10. Even after the gamma-ray emission at  $R \sim \Gamma^2 c \Delta t$  (the time-delay  $\Delta t \sim 0.4$  s between gamma-ray and GW), a significant amount of the kinetic energy ( $\sim 10^{49}$  erg) may remain as an outflow, which plunges into the ambient medium. Similarly to the model for the NS-NS merger (Piran, Nakar & Rosswog 2013), we can expect an afterglow emission from the forward shock formed by the outflow especially in the radio band.

### 3. Afterglows

Bulk of gamma-ray emitting materials push ambient medium to form a shock, generating high-energy electrons which produce synchrotron radiation. We calculate such afterglows in the same procedure to those of GRBs (Piran 1999; Zhang & Mészáros 2004; Kumar & Zhang 2015). Initially the ejecta mass  $M_{\text{ej}}$  are injected at the origin  $r = 0$  with expanding bulk Lorentz factor  $\gamma_0$ . The burst energy is then  $E_0 = \gamma_0 M_{\text{ej}} c^2$ , with which the material expands outwards. As will be shown later, given the energy  $E_0$ , the parameter  $\gamma_0$  only affects the very early stage of the afterglow. The uncertainty in  $\gamma_0$  does not disturb the prediction of the late afterglow, which may be detected in the future. We assume spherical expansion — jet

collimation is not considered (see section 4 for discussion). The ambient matter is uniform with the density  $n_0$ . Following the previous work of Huang et al. (2000), the dynamics of the shock is numerically computed. In deriving the observed flux density of the synchrotron emission  $F_\nu$  at frequency  $\nu$ , we integrate emissivity over the equal arrival time surface (e.g., Granot et al. 1999; Huang et al. 2000), assuming thin shell emission approximation. Using standard convention in GRB community, the power-law index of the electron distribution  $p$ , together with the microphysics parameters  $\epsilon_e$  and  $\epsilon_B$ , determines the emissivity profile in the comoving frame. In calculating the radio synchrotron emission, we take into account the effect of synchrotron self-absorption (SSA). Optical depth  $\tau_a(\nu)$  to SSA was given by, for example, Eq. (52) of Panaitescu & Kumar (2000). Self-absorption frequency  $\nu_a$ , at which  $\tau_a(\nu_a)$ , is generally below the radio band, so that the emission is optically thin. We adopt  $E_0 = 1 \times 10^{49}$  erg,  $\gamma_0 = 10$ ,  $p = 2.3$ ,  $n_0 = 1 \text{ cm}^{-3}$ ,  $\epsilon_e = 0.1$ ,  $\epsilon_B = 0.01$ , and  $z = 0.09$  as fiducial parameters.

Red curves in Figure 1 show afterglow light curves at 1.4 GHz radio band for fiducial parameters. The flux initially increases and there is a small bump at  $t \approx 3 \times 10^5$  sec after the GW event. Around this time, the decreasing absorption frequency  $\nu_a$  crosses both the observation frequency of 1.4 GHz and the minimum frequency  $\nu_m$ , which is the characteristic frequency of the synchrotron emission by electrons with the minimum Lorentz factor  $\gamma_m$ . When  $t \gtrsim 10^7$  sec, the flux increases again. This behavior is analytically confirmed as follows. At  $t = 5.5 \times 10^5$  sec, the shock reaches the radius at which  $\gamma\beta = 1$ , where  $\beta$  is the shock velocity divided by the velocity of light and  $\gamma = (1 - \beta^2)^{-1/2}$ . After that, the expansion velocity becomes Newtonian. Furthermore, we can see  $\gamma_m \ll \gamma_a \ll \gamma_c$  if  $t > 3 \times 10^6$  sec, where  $\gamma_a$  is the electron Lorentz factor at which  $\tau_a = 1$ , and  $\gamma_c$  is the electron Lorentz factor above which synchrotron cooling is significant. Finally, if  $t > 3 \times 10^7$  sec, then the shock dynamics is well approximated by the scaling of Sedov solution ( $\beta \propto t^{-3/5}$ ) and  $\gamma_m$  is of order unity. In this case, one can see  $\gamma_a \propto [m(r)/r^2 B]^{1/(p+4)}$ , where  $B$  and  $m(r)$  are the magnetic field strength in the comoving frame and the swept-up mass of ambient matter at the shock radius  $r$ , respectively. Using the non-relativistic Sedov scalings,  $r \propto t^{2/5}$ ,  $m(r) \propto r^3 \propto t^{6/5}$ , and  $B \propto \beta \propto t^{-3/5}$ , we obtain  $\gamma_a \propto t^{1/(p+4)}$  and  $\nu_a \propto \gamma_a^2 B \propto t^{-(3p+2)/(5p+20)}$ . Hence, we derive  $F_\nu \propto m(r)B(\nu/\nu_a)^{-(p-1)/2} \propto t^\alpha \nu^{-(p-1)/2}$ , where  $\alpha = (-3p^2 + 7p + 26)/(10p + 40)$  — namely  $\alpha = 0.416$  for  $p = 2.3$ .

One can see the parameter dependence from Figure 1. Changes of  $\gamma_0$  only affects the flux at very early epoch. For smaller value of  $p$ , the radio flux at  $t \gtrsim 10^7$  sec is larger. The number density of the ambient matter is highly uncertain, so that we take the wide range of  $n_0$  in showing Figure 2. The radio emission is brighter for larger  $n_0$ .

Figures 2 shows optical R-band light curves, similarly to Figure 1. Overall qualitative

behavior looks similar to that of radio emission, while optical bumps are more significant and earlier. The peak epoch of the bump roughly corresponds to the onset time of deceleration of the outflow (Sari & Piran 1999), which is estimated as  $t_{\text{dec}} = (3E_0/32\pi\gamma_0^8 n_0 m_p c^5)^{1/3} = 4.2 \times 10^3$  sec for our fiducial parameters. One can recognize again the flux increasing at late epoch  $t \gtrsim 10^7$  sec.

#### 4. Discussions

Radio follow-up observations of GW150914 might be done or on-going with typical sensitivity of around a few tens of  $\mu\text{Jy}$  at 1.4 GHz. The radio observations will be able to constrain the number density of the ambient matter (see the right panel of Figure 1). If the radio afterglow is not detected at later epoch ( $t \gtrsim 10^6$  sec), the ambient density  $n_0$  may be smaller than  $\sim 10^{-1} \text{ cm}^{-3}$ . Optical/infrared upper limits have also been given (Annis et al. 2016; Soares-Santos et al. 2016; Smartt et al. 2016). Typical survey depth is  $\sim 20\text{--}22$  mag, corresponding to  $\sim 10\text{--}30 \mu\text{Jy}$ , which is well above the prediction of our afterglow model. Hence the reported optical/infrared non detections do not constrain our model parameters. Upper limits at very early epoch ( $t \lesssim 10^4$  sec) would have given the upper bound of  $\gamma_0$  (see Figure 3). Note that for  $p \lesssim 2.2$ , the optical/infrared afterglows are expected to be still detectable with large telescopes such as Subaru Hyper Suprime-Cam<sup>1</sup>. Further follow-up observations are encouraged.

We briefly comment on the X-ray flux of the afterglow. Our model predicts that for  $t \gtrsim 10^5$  sec, the X-ray flux is below  $10^{-14} \text{ erg s}^{-1}\text{cm}^{-2}$  for fiducial parameters. *Swift* XRT started follow-up observation about 2 days after the GW trigger, and no X-ray counterpart was detected (Evans et al. 2016). The flux upper limit is  $6 \times 10^{-13}\text{--}10^{-11} \text{ erg s}^{-1}\text{cm}^{-2}$ . The model prediction is then well below this upper limit, so that our afterglow model is not constrained.

In this paper, we have considered spherically symmetrical outflow. Data analysis of GW showed that inclination angle, which is the angle between the total angular momentum and the line of sight, may be large ( $\gtrsim 30$  deg) although uncertainty is large (LIGO Scientific Collaboration and V

---

<sup>1</sup> <http://www.naoj.org/Projects/HSC/index.html>

brighter radio emission. Furthermore, on-axis emission would have unusually high typical photon energy.

This work was supported in part by a Grant-in-Aid for Scientific Research of the Japanese Ministry of Education, Culture, Sports, Science and Technology, No.15K05088 (R.Y.), No. 25400227 (K.A.).

## REFERENCES

Abbott, B. P. et al. (LIGO Scientific Collaboration and Virgo Collaboration) 2016, PRL, 116, 061102

Annis, J. et al. 2016, arXiv:1602.04199

Blandford, R. D., & Znajek, R. L. 1977, MNRAS, 179, 433

Connaughton, V. et al. 2016, arXiv:1602.03920

Evans, P. A. et al. 2016, arXiv:1602.03868

Fermi LAT Collaboration 2016, arXiv:1602.04488

Granot, J. Piran, T. & Sari, R. 1999, ApJ, 513, 679

Huang, Y. F. et al. 2000, ApJ, 543, 90

Kumar, P., & Zhang, B. 2015, Phys. Rep., 561, 1

The LIGO Scientific Collaboration and The Virgo Collaboration 2016, arXiv:1602.03840

Panaitescu, A. & Kumar, P. 2000, ApJ, 543, 66

Piran, T. 1999, Phys. Rep., 314, 575

Piran, T., Shemi, A., & Narayan, R., 1993, MNRAS, 263, 861

Piran, T., Nakar, E., & Rosswog, S. 2013, MNARS, 430, 2121

Planck Collaboration 2015, arXiv:1502.01589

Sari, R. & Piran, T. 1999, ApJ, 520, 641

Savchenko, V. et al. 2016, arXiv:1602.04180

Shemi, A. & Piran, T. 1990, ApJ, 365, L55

Soares-Santos, M. et al. 2016, arXiv:1602.04198

Smartt, S. J. et al. 2016, arXiv:1602.04156

Thompson, C. & Duncan, R. C. 1995, MNRAS, 275, 255

Yamazaki, R. et al. 2002, ApJL, 571, L31

Yamazaki, R. et al. 2004, ApJL, 606, L33

Zhang, B., & Mészáros, P. 2004, International Journal of Modern Physics A, 19, 2385

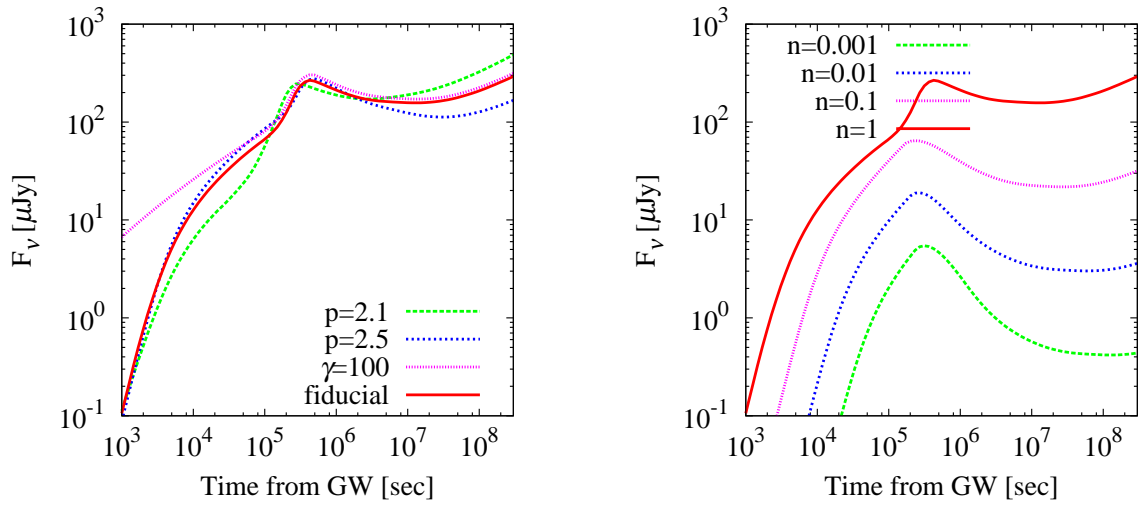


Fig. 1.— Radio afterglow light curves at 1.4 GHz. The red curves in both panels are for fiducial parameters ( $E_0 = 1 \times 10^{49}$  erg,  $\gamma_0 = 10$ ,  $p = 2.3$ ,  $n_0 = 1 \text{ cm}^{-3}$ ,  $\epsilon_e = 0.1$ ,  $\epsilon_B = 0.01$ , and  $z = 0.09$ ). (Left panel) Green, blue, and purple curves are for  $p = 2.1$ ,  $p = 2.5$ , and  $\gamma_0 = 100$  with the other parameters fixed at their fiducial values. (Right panel) Green, blue, and purple curves are for  $n_0 = 0.001$ ,  $0.01$ , and  $0.1 \text{ cm}^{-3}$  with the other parameters fixed at their fiducial values.

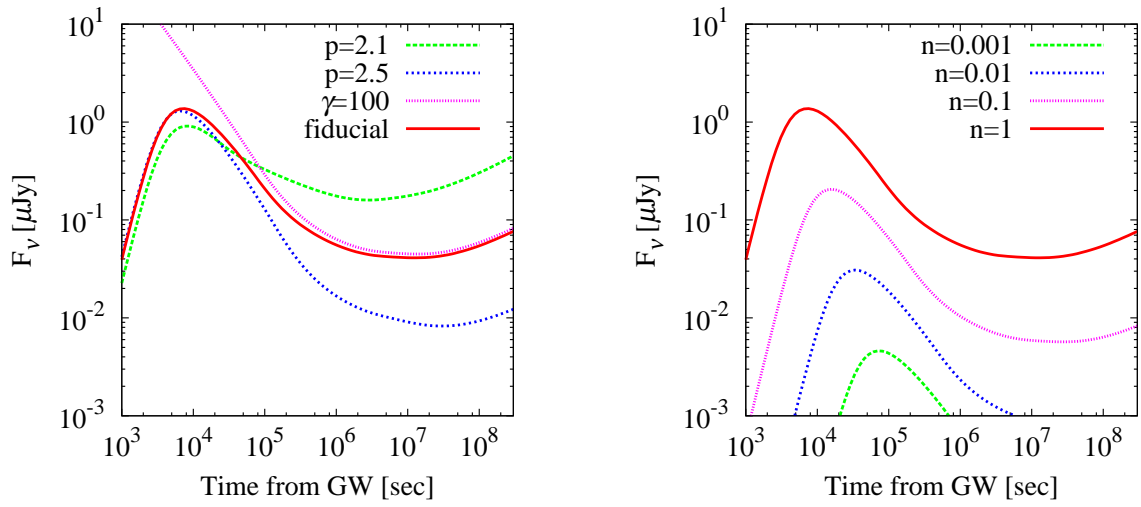


Fig. 2.— Optical afterglow light curves at R-band. The red curves in both panels are for fiducial parameters ( $E_0 = 1 \times 10^{49}$  erg,  $\gamma_0 = 10$ ,  $p = 2.3$ ,  $n_0 = 1 \text{ cm}^{-3}$ ,  $\epsilon_e = 0.1$ ,  $\epsilon_B = 0.01$ , and  $z = 0.09$ ). (Left panel) Green, blue, and purple curves are for  $p = 2.1$ ,  $p = 2.5$ , and  $\gamma_0 = 100$  with the other parameters fixed at their fiducial values. (Right panel) Green, blue, and purple curves are for  $n_0 = 0.001$ ,  $0.01$ , and  $0.1 \text{ cm}^{-3}$  with the other parameters fixed at their fiducial values.